

Detecting the Saliency of Remote Sensing Images Based on Sparse Representation of Contrast-weighted Atoms

Zhou Huang^a, Huai-Xin Chen^{a,*}, Yun-Zhi Yang^b, Chang-Yin Wang^b,
Bi-Yuan Liu^a

^aUniversity of Electronic Science and Technology of China, Chengdu, China

^bCETC Special Mission Aircraft System Engineering Co.Ltd, Chengdu, China

Abstract

Object detection is an important task in remote sensing (RS) image analysis. To reduce the computational complexity of redundant information and improve the efficiency of image processing, visual saliency models are gradually being applied in this field. In this paper, a novel saliency detection method is proposed by exploring the sparse representation (SR) of, based on learning, contrast-weighted atoms (LCWA). Specifically, this paper uses the proposed LCWA atom learning formula on positive and negative samples to construct a saliency dictionary, and on nonsaliency atoms to construct a discriminant dictionary. An online discriminant dictionary learning algorithm is proposed to solve the atom learning formula. Then, we measure saliency by combining the coefficients of SR and reconstruction errors. Furthermore, under the proposed joint saliency measure, a variety of salient maps are generated by the discriminant dictionary. Finally, a fusion method based on global gradient optimisation is proposed to integrate multiple salient maps. Experimental results show that the proposed method significantly outperforms current state-of-the-art methods under six evaluation measures.

Keywords: Contrast-weighted atom, Dictionary learning, Gradient optimisation, Road detection, Saliency detection

*Corresponding author.

Email addresses: chowhuang23@gmail.com (Zhou Huang),
huaixinchen@uesct.edu.cn (Huai-Xin Chen), yangyz@cetca.net.cn (Yun-Zhi Yang),
wangcy@cetca.net.cn (Chang-Yin Wang), lby9469@163.com (Bi-Yuan Liu)

1. Introduction

Guided by our attention, the human visual system (HVS) can quickly and automatically select regions of interest in complex scenes (called visual saliency) [1]. This intelligent mechanism of the HVS has been extensively studied in the fields of psychology [2], neurobiology [3], and computer vision [4, 5]. In the past two decades, research on visual saliency has advanced in two ways: eye fixation prediction in human vision [6] and salient target detection in computer vision [7, 8, 9]. The former focuses on predicting the eye fixations of the observer in a short time [10], whereas the latter tends to locate or segment the most prominent objects in the scene [11, 12, 13]. Because saliency detection can optimise the computing resources required for image analysis, visual saliency models are widely used in various fields of remote sensing (RS) image processing, including regions of interest extraction [14], regional change detection [15], and adaptive image fusion [16].

The latest research [17] proposes that information is always represented by a few simultaneously active neurons. The retina receives much information, whereas only a small amount of effective information is transmitted to nerve cells in the visual cortex for processing. This information representation can be called sparse representation (SR) [18]. The principle of SR is to represent the signal by a linear combination of a series of base vectors in the overcomplete dictionary, and that linear combination is required to be sparse [19]. In recent years, image structure analysis based on sparse representation has been widely used in computer vision and image processing (such as image fusion [20], image classification [21] and image restoration [22]). Simultaneously, SR theory has been introduced into the field of image saliency detection [10, 23, 24]. However, there are two key problems with SR-based salient object detection methods: the construction of the SR dictionary and the criteria for saliency measure.

In the construction of dictionaries, most of the early methods used the independent component analysis (ICA) method to sample many image patches from various kinds of natural images to generate basic atoms [25, 26]. However, these basic atoms cannot make a perfect SR of the detection image without information loss because some features of the training image cannot be accurately captured by the predetermined basic atom. Other SR-based methods [27, 28] usually use the patches around the detected patches for dictionary construction. However, as [29] showed, when the salient object has a high contrast with the surrounding patches, such methods usually assign

higher values to the edges of the salient object rather than the entire object. Recently, background prior [30] was introduced into the SR-based saliency detection methods, which assumes that nonsaliency parts of the image are usually distributed on the boundary. Under this assumption, patches or superpixels near the boundaries of the image are usually selected to build the background dictionary [31, 32, 33]. However, when the salient object is near the image boundary, some foreground regions are included in the background dictionary, which causes them to be mistakenly detected as background regions. Also, if the background regions far away from the image boundary and the background regions near the image boundary have obvious characteristics, some background regions will also be incorrectly marked as foreground. Moreover, the training sample patches usually have their own features, such as intensity and contrast, but the features of those samples are usually disregarded in most existing saliency object detection methods, resulting in saliency objects in a scene with similar background and foregrounds not being evenly highlighted.

In terms of saliency measurement criteria, a saliency detection method based on SR defines saliency measurement by reconstruction error or by the sparsity of representation coefficients (that is, using l_0 -norm to calculate coding length) [10, 23, 24, 31, 34]. Also, those methods usually add sparse constraints to sparse coefficients to achieve sparse coding of image patches, and they calculate the saliency of image patches by minimising the sum of the reconstruction errors. Therefore, that representation method is more sensitive to non-Gaussian noise rather than outliers representing coefficients [31].

Through our research, we found that two or more temporary saliency maps are generated in most saliency detection models. Among those methods, some methods determine the fusion weights through simple weights [24, 31] or experimental effects [10, 35, 36]. Other methods determine the optimal image fusion weights through methods such as least-squares estimation of training data [37] or Bayesian inference [23], but those methods do not consider the connections between multiple saliency maps.

To solve the above problems, we propose an SR method based on learning contrast-weighted atoms (LCWA) for road saliency detection in RS images. More specifically, this study used positive and negative samples of RS images including roads as the template for dictionary learning. We propose a new contrast-weighted formula in the dictionary learning process for learning two enhanced discriminant dictionaries from positive and negative sam-

ple patches, which improves the contribution of the features of the sample patches themselves to the entire dictionary. On the basis of the online dictionary learning algorithm [19], to solve the problem of dictionary learning we also propose an online discriminant contrast-weighted dictionary learning (CWDL) algorithm based on contrast weights, which effectively overcomes the shortcomings of some methods using background priors. Then, in our study, the test image patches were sparsely represented one by one by the learned discriminant dictionary.

To measure saliency, we used l_2 -norm to measure the sparsity of sparse coefficients and combined $l_{1,2}$ -norm to calculate the sparse reconstruction errors to improve the expression of outliers in the sparse coefficient. For multiple salient maps generated by calculating representation coefficients, we propose an image fusion method based on global gradient optimisation to integrate multiple salient images. To summarise, the main contributions of this paper are as follows:

- (1) Considering the features of the training sample patch itself, we propose a novel atomic learning formula based on contrast weights. Also, we used an online discriminative CWDL to solve the formula.
- (2) We used the l_2 -norm to measure the sparsity of sparse coefficients, used the $l_{2,1}$ -norm measure to sparse the reconstruction errors, and then combined the two measures to improve the expression of outliers in the representation coefficients.
- (3) We used a salient map fusion method based on global gradient optimisation to integrate multiple saliency maps. This method optimised the image fusion effect by establishing the relation between saliency maps.

The rest of this paper is organised as follows: Section 2 briefly reviews related work. Section 3 describes the method of salient target detection in detail. Sections 4 and 5 give the experimental analysis and conclusions.

2. Related work

In recent years, more and more researchers are committed to the work of salient object detection [23, 38, 39, 40]. Some of the review papers [1, 4, 5] have investigated and discussed many of the most advanced saliency target detection methods in detail. In this section, we review the work that was

most relevant to us, including SR-based saliency object detection and the application of saliency detection in optical RS images. Also, salient object detection based on red-green-blue depth (RGB-D) is also a research hotspot in recent years and will be briefly reviewed in this section.

2.1. Salient object detection method based on sparse representation

In recent years, the SR theory has been gradually addressed in the field of saliency detection. Generally, SR based saliency detection methods need to construct an overcomplete dictionary first, sparsely represent the input image through the dictionary, and then measure the saliency according to the SR coefficients or reconstruction errors. In [10] and [41], the construction of the dictionary was learned by doing ICA on the image patches sampled from each position of the current input image and using the reconstruction errors to measure the saliency. In the methods of [27] and [42], the image patches around the central patch were used to do SR, and the saliency was measured by coding length or residual. Those methods usually gave higher saliency values to the object boundaries, because both the background and foreground are included in the dictionary.

Later, the background prior method [30] was proposed. On the basis of that assumption, some methods [32, 33] used patches or superpixels near the image boundary as background templates to construct a global background dictionary to reconstruct the image sparsely. Recently, in [43] a compact background dictionary was constructed for sparse reconstruction so that the background region could be reconstructed well. In [44], a saliency target detection method was proposed based on two-stage graphs, taking into account the consistency of adjacent spaces between graph nodes and the consistency of regional space, while improving the accuracy of saliency target detection in complex scenes.

2.2. Application of saliency object detection in a remote sensing image

Due to the rapid development of massive RS data and the complexity of RS scenes, many traditional methods of processing natural images are not suitable for RS images. As one method of data compression and rapid screening, saliency detection can effectively process RS data, and there are essential similarities between saliency object detection and target detection and extraction in RS images. They both extract regions of interest in an image based on the saliency of a particular task or target. As image processing and RS technology have developed, saliency detection-based methods have

been widely used in the field of RS. Many researchers combine visual saliency and image interpretation to accomplish specific target detection, such as airport detection [45], building detection [46], oil tank detection [47], and ship detection [48]. Yao et al. [45] proposed a coarse-to-fine airport saliency detection model. At the coarse layer, combined with clues of contrast and linear density, a goal-oriented saliency model was established to quickly locate airport candidate regions. Then, Li [47] et al. proposed a two-step building extraction method based on saliency cues, designed a saliency estimation algorithm for building objects, extracted saliency cues in a local region of each candidate building, and integrated them into a probability model to get the final building extraction results. In [49], texture saliency and color saliency were integrated into pixel-level saliency mapping to extract regions of interest. However, those methods did not involve road detection methods based on saliency RS images.

2.3. RGB-D saliency detection

When dealing with complex scenes, such as similar foreground and background, multiple or transparent objects, cluttered backgrounds, or low-contrast environments, traditional RGB-based saliency detection methods may fail [5, 9, 30, 36, 39]. Depth cues with abundant spatial structures and 3-D layout information can contribute to handling those cases. RGB-D saliency detection methods can be divided into two categories according to the selection of features: manually designing hand-crafted features and automatic feature extraction using convolutional neural networks (CNNs). For the first category, [50] combined the saliency generated by RGB with the saliency of depth information and proposed a new multistage saliency target detection model. [51] proposed a new method of salient target detection surrounded by a local background. [52] proposed an anisotropic centre-bounded difference. Those methods relied mainly on the features of manual construction and a lack of high-level representation. In the second category, [53] used hand-made features to train CNN-based models and achieved marked improvements over traditional methods. In [54], a fusion network was designed in which cross-layer features were gradually combined, and better performance was obtained. In some recent work, [55] introduced the contrast prior information of the saliency detection method of nondeep learning into the CNN-based architecture to enhance depth information. [56] combined depth cues with multiscale contextual features and proposed a new depth-guided multiscale recursive attention network to achieve the precise locations of salient

targets. In [57], they first constructed a 1 K high-resolution saliency person dataset, then systematically summarised 31 popular models, and finally proposed a baseline architecture called a Deep Depth-Depurator Network for saliency detection.

3. Proposed saliency detection method

This section describes the proposed saliency target detection method in detail. As shown in Fig. 1, the method includes three main parts: CWDL-based discriminant dictionary learning, salient image generation, and salient image fusion.

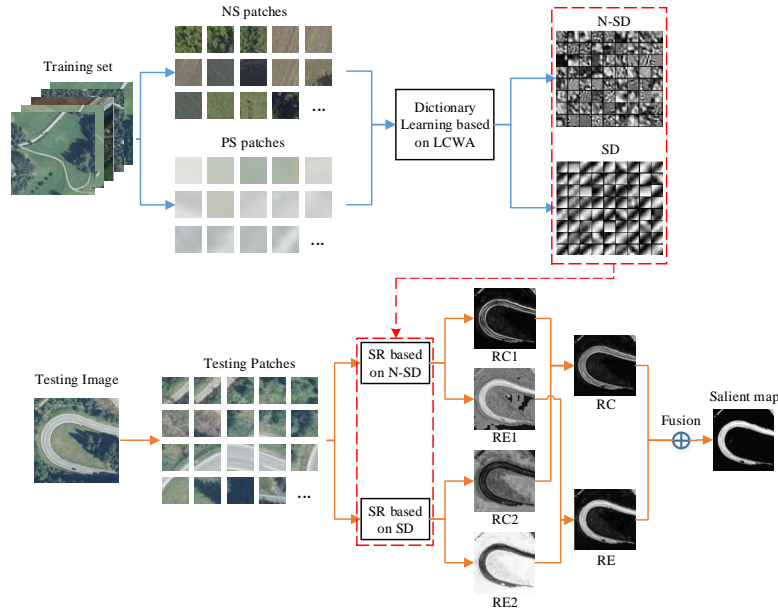


Figure 1: Diagram of the proposed salient object detection method. NS, negative sample; PS, positive sample; N-SD, nonsalient dictionary; SD, salient dictionary; SR, sparse representation; RC, representation coefficient; RE, reconstruction error.

3.1. Contrast-weighted dictionary learning formula

In the image processing method based on SR, an image patch is usually represented by a linear combination of a few atoms in an overcomplete dictionary $\mathbf{D} = \{\mathbf{d}_i\}_{i=1}^k \in \mathbb{R}^{n \times k}$, that is, the image patch $\mathbf{x} \in \mathbb{R}^n$ is estimated by dictionary \mathbf{D} and the calculated sparse coefficients $\boldsymbol{\alpha} \in \mathbb{R}^k$. The equation is

$$\mathbf{x} = \mathbf{D}\boldsymbol{\alpha} \quad s.t. \quad \|\mathbf{x} - \mathbf{D}\boldsymbol{\alpha}\|_2 \leq \xi, \quad (1)$$

where $\|\bullet\|_2$ is the l_2 -norm used to measure the deviation and ξ is the error. Within the feasible set, the solution that minimises the number of nonzero sparse coefficients is undoubtedly an attractive representation. This most SR is

$$\min_{\boldsymbol{\alpha} \in \mathbb{R}^k} \|\mathbf{x} - \mathbf{D}\boldsymbol{\alpha}\|_2^2 \quad s.t. \quad \|\boldsymbol{\alpha}\|_0 \leq L, \quad (2)$$

where L is the sparsity of the coefficients $\boldsymbol{\alpha}$. In Eq. 2, the atoms in \mathbf{D} represent the smallest unit in the reconstructed image patch. Here, the atoms in \mathbf{D} need to be learned from the training patches $\mathbf{X} = \{\mathbf{x}\}_{i=1}^m$, which can be achieved by [19]

$$\min_{\mathbf{D}, \mathbf{A}} \frac{1}{m} \sum_{i=1}^m \left(\frac{1}{2} \|\mathbf{x}_i - \mathbf{D}\boldsymbol{\alpha}_i\|_2^2 + \lambda \|\boldsymbol{\alpha}_i\|_1 \right), \quad (3)$$

where λ is the trade-off between the reconstruction errors $\|\mathbf{x}_i - \mathbf{D}\boldsymbol{\alpha}_i\|_2^2$ and the sparsity of the coefficient $\|\boldsymbol{\alpha}_i\|_1$ and $\mathbf{A} = \{\boldsymbol{\alpha}_i\}_{i=1}^m$ is the SR coefficients set corresponding to \mathbf{X} . According to Eq. 3, we studied salient dictionary and nonsalient dictionary learning based on contrast-weighted atoms. As one of the features of an image, contrast plays an important role in both local-based and global-based saliency detection methods [36, 55, 58]. Accordingly, we added a new contrast weight to the dictionary learning formula to strengthen or weaken the salient or nonsalient atoms of learning.

More specifically, in our weight function, the weight of each pixel of the basic atom was determined by the brightness contrast weight of all the image patches in the corresponding sample patches relative to the training set $\mathbf{X}^H = \{\mathbf{X}^N \cup \mathbf{X}^P\}$, where P and N are the identification of the positive and negative sample set respectively. The weight of the i -th training sample patches is expressed as

$$\mathbf{w}(\mathbf{x}_i) = \frac{Lum(\mathbf{x}_i) - \text{mean}(Lum(\mathbf{X}^H))}{\max(Lum(\mathbf{X}^H))}, \quad (4)$$

where $Lum(\bullet)$ is the luminance value operator for calculating the sample patch, and similarly $\text{mean}(\bullet)$ and $\max(\bullet)$ are the average value operator and the maximum value operator respectively. Note that in the actual calculation, the sample patch is treated as a column vector; that is, $\mathbf{w}(\mathbf{x}_i)$ can be expressed as $\mathbf{w}_i^T \in \mathbb{R}^{1 \times n}$, and n is the number of pixels of the sample patch. According to $\mathbf{W}^T \in \{\mathbf{w}_i^T\}_{i=1}^m$, the contrast weight term can be expressed as

$\|\mathbf{W}_i^T \mathbf{D}\|_2^2$. So given the contrast weight term, by rewriting Eq. 3, we have the following salient and nonsalient dictionaries to learn the optimisation equation:

$$\min_{\mathbf{D}^H, \mathbf{A}^H} \frac{1}{m^H} \sum_{i=1}^{m^H} \left(\frac{1}{2} \|\mathbf{x}_i^H - \mathbf{D}^H \boldsymbol{\alpha}_i^H\|_2^2 + \lambda_1 \|\boldsymbol{\alpha}_i^H\|_1 + \lambda_2 \|\mathbf{W}_i^T \mathbf{D}^H\|_2^2 \right), \mathbf{H} = \{ \text{P} \vee \text{N} \}, \quad (5)$$

where m^H represent the number of positive or negative samples, $\{\boldsymbol{\alpha}_i^H\}_{i=1}^{m^H}$ is the SR coefficient of positive or negative sample patches, and \mathbf{D}^H is a salient dictionary or nonsalient dictionary trained from positive or negative samples. The meaning of λ_1 is the same as that of λ in formula (3), λ_2 (a very small positive number) is a regularisation parameter that controls the influence of contrast weighting terms.

3.2. The solution to the dictionary learning formulation

We can learn the salient dictionary and the nonsalient dictionary through (5). Because the online dictionary learning algorithm [19] can deal with large dynamic datasets and is faster than the batch algorithm, we propose the CWDL algorithm to solve (5). Consistent with the usual dictionary learning algorithm, we divided the optimisation problem in (5) into two subprocesses to solve alternately; namely, SR and dictionary update. Specifically, generally the initialisation training dictionary \mathbf{D}^H is obtained by randomly sampling the training sample set. So the first step was to fix \mathbf{D}^H , the sparse coefficient $\mathbf{A}^H = \{\boldsymbol{\alpha}_i^H\}_{i=1}^{m^H}$ could be obtained by the SR method. The second step was to fix \mathbf{A}^H , and the updated dictionary \mathbf{D}^H could be solved by the dictionary update method. The first and second steps of the iteration were done until the convergence condition was reached.

3.2.1. Sparse representation

From the above, it can be seen that the solution of (5) was an iterative optimisation process, assuming that in the i -th iteration, \mathbf{x}_t^H is a randomly selected image patch from the training set, and $\boldsymbol{\alpha}_t^H$ is the coefficient of \mathbf{x}_t^H obtained by the $(t-1)$ -th updated dictionary \mathbf{D}_{t-1}^H through the SR algorithm. Because the contrast-weighted term $\lambda_2 \|\mathbf{W}_i^T \mathbf{D}^H\|_2^2$ in (5) is independent of the sparse coefficient $\boldsymbol{\alpha}_i^H$, the sparse coefficient $\boldsymbol{\alpha}_i^H$ in the i -th iteration can be

expressed as

$$\boldsymbol{\alpha}_t^H \triangleq \arg \min_{\boldsymbol{\alpha}_t^H \in \mathbb{R}^k} \frac{1}{2} \|\mathbf{x}_t^H - \mathbf{D}_{t-1}^H \boldsymbol{\alpha}_t^H\|_2^2 + \lambda_1 \|\boldsymbol{\alpha}_t^H\|_1, \quad (6)$$

The SR problem of the above fixed dictionary is the l_1 -regularised linear least square problem. In this paper, the LARS-Lasso algorithm [59] is used to solve this problem.

3.2.2. Dictionary update

After the SR step of the t -th iteration, the sparse coefficient $\{\alpha_i^H\}_{i=1}^t$ of the image patch $\{\mathbf{x}_i^H\}_{i=1}^t$ after training is obtained. In the t -th iteration, fixed α_i^H , the dictionary be updated by the following optimization function according to (5):

$$\mathbf{D}_t^H \triangleq \arg \min_{\mathbf{D}_t^H \in \mathbb{R}^{n \times k}} \frac{1}{t} \sum_{i=1}^t \left(\frac{1}{2} \|\mathbf{x}_i^H - \mathbf{D}_{t-1}^H \boldsymbol{\alpha}_i^H\|_2^2 + \lambda_1 \|\boldsymbol{\alpha}_i^H\|_1 + \lambda_2 \|\mathbf{W}^T \mathbf{D}_{t-1}^H\|_2^2 \right), \quad (7)$$

where \mathbf{D}_t^H is the discriminant dictionary obtained after the t -th iterative learning.

Because the patch coordinate descent algorithm [60] has the advantages of no parameters and no need for any learning rate adjustment, we updated each atom of the dictionary through this algorithm. For example, the j -th atom $\mathbf{d}_{j,t}^H$ of updating the dictionary in the t -th iteration is calculated by

$$\mathbf{d}_{j,t}^H = \mathbf{d}_{j,t-1}^H - \frac{\sigma}{t} \frac{\partial}{\partial \mathbf{d}_j^H} \left[\sum_{i=1}^t \left(\frac{1}{2} \|\mathbf{x}_i^H - \widehat{\mathbf{D}}_{j,t}^H \boldsymbol{\alpha}_i^H\|_2^2 + \lambda_1 \|\boldsymbol{\alpha}_i^H\|_1 + \lambda_2 \|\mathbf{w}_j^T \widehat{\mathbf{D}}_{j,t}^H\|_2^2 \right) \right]_{|\mathbf{d}_{j,t-1}^H}. \quad (8)$$

For convenience, let

$$\mathbf{M} = \sum_{i=1}^t \left(\frac{1}{2} \|\mathbf{x}_i^H - \widehat{\mathbf{D}}_{j,t}^H \boldsymbol{\alpha}_i^H\|_2^2 + \lambda_1 \|\boldsymbol{\alpha}_i^H\|_1 + \lambda_2 \|\mathbf{w}_j^T \widehat{\mathbf{D}}_{j,t}^H\|_2^2 \right). \quad (9)$$

In Eq. 8, σ is the learning rate of gradient descent, $\widehat{\mathbf{D}}_{j,t}^H = [\mathbf{d}_{1,t}^H, \mathbf{d}_{2,t}^H, \dots, \mathbf{d}_{j,t}^H, \mathbf{d}_{j+1,t-1}^H, \dots, \mathbf{d}_{k,t-1}^H]$, Noted that only $\mathbf{d}_{j,t}^H$ in $\widehat{\mathbf{D}}_{j,t}^H$ is a variable that must

be updated. After Eq. 8 the current iteration, the previous j atoms, that is, $\{\mathbf{d}_{1,t}^H, \mathbf{d}_{2,t}^H, \dots, \mathbf{d}_{j,t}^H\}$, are updated. Using the trace $Tr(\bullet)$ of the matrix to represent the l_2 -norm and then expressing it as the derivative about \mathbf{d}_j^H , Eq. 9 can be rewritten as

$$\begin{aligned} \frac{\partial}{\partial \mathbf{d}_j^H} (\mathbf{M})|_{\mathbf{d}_{j,t-1}^H} &= \frac{1}{2} \frac{\partial}{\partial \mathbf{d}_j^H} Tr \left[\left(\widehat{\mathbf{D}}_{j,t}^H \right)^T \widehat{\mathbf{D}}_{j,t}^H \mathbf{B}_t^H \right] - \frac{\partial}{\partial \mathbf{d}_j^H} Tr \left[\left(\widehat{\mathbf{D}}_{j,t}^H \right)^T \mathbf{C}_t^H \right] \\ &\quad + \frac{\partial}{\partial \mathbf{d}_j^H} Tr \left[\lambda_2 t \mathbf{W}_j^T \widehat{\mathbf{D}}_{j,t}^H \left(\widehat{\mathbf{D}}_{j,t}^H \right)^T \mathbf{W}_j \right], \end{aligned} \quad (10)$$

where \mathbf{B}_t^H and \mathbf{C}_t^H are defined as $\sum_{i=1}^t \alpha_i^H (\alpha_i^H)^T$ and $\sum_{i=1}^t \mathbf{x}^H (\alpha_i^H)^T$, which refer to storing all the information of the sparse coefficients and sparsely represented image patches of all previous iterations respectively. According to the derivative calculation rule of matrix trace, Eq. 10 can be expressed as

$$\frac{\partial}{\partial \mathbf{d}_j^H} (\mathbf{M})|_{\mathbf{d}_{j,t-1}^H} = \widehat{\mathbf{D}}_{j,t}^H \mathbf{b}_{j,t}^H - \mathbf{c}_{j,t}^H + 2\lambda_2 t \mathbf{W}_j \mathbf{W}_j^T \mathbf{d}_j^H, \quad (11)$$

where $\mathbf{b}_{j,t}^H$ and $\mathbf{c}_{j,t}^H$ represent the j -th columns of $\mathbf{B}_{j,t}^H$ and $\mathbf{C}_{j,t}^H$ respectively. So Eq. 8 can be rewritten as

$$\mathbf{d}_{j,t}^H = \mathbf{d}_{j,t-1}^H - \frac{\sigma}{t} \left(\widehat{\mathbf{D}}_{j,t}^H \mathbf{b}_{j,t}^H - \mathbf{c}_{j,t}^H \right) - 2\lambda_2 \sigma \mathbf{W}_j \mathbf{W}_j^T \mathbf{d}_{j,t-1}^H. \quad (12)$$

According to [19], the σ/t in Eq. 12 can be expressed approximately as $1/\mathbf{B}_j^H(j, j)$. When all the atoms $\{\mathbf{d}_{j,t}^H\}_{j=1}^k$ are updated, the dictionary \mathbf{D}_t^H completes the t -th learning.

In summary, after iterative SR and dictionary update steps, we get salient dictionaries and nonsalient dictionaries. Table 1 summarises our CWDL algorithm.

3.3. Saliency image generation

This subsection describes the saliency measurement criteria based on SR coefficients and reconstruction errors.

3.3.1. Saliency measure based on sparse representation coefficients

In the saliency detection process, the saliency of each pixel can be measured to a certain extent by the representation coefficient of an image patch centered on the pixel. As shown in Fig. 2, when sparsely reconstructed from a

Table 1: Summary of the CWDL algorithm

Algorithm 1. Online discriminant dictionary learning algorithm based on contrast weighting

Input: Vectorised training patches $\mathbf{X}^H \in \mathbb{R}^{n \times m}$.
Output: The learned dictionary $\mathbf{D}^H \in \mathbb{R}^{n \times k}$.
Initialization: The contrast-weighted matrix \mathbf{W}^T is obtained by Eq. 4;
Randomly select the samples in the training set to fill \mathbf{D}_0^H ;
Set $\mathbf{B}_0^H \in \mathbb{R}^{k \times k}$ and $\mathbf{C}_0^H \in \mathbb{R}^{n \times k}$ to zero matrices;
Regularization parameter λ_1 and λ_2 ;
Number of iterations T .

1. **For** $t = 1$ to T **do**
2. Randomly select the image patches \mathbf{X}^H from the training set $\mathbf{x}_t^H \in \mathbb{R}^{k \times 1}$.
3. Sparse coding:
Obtained $\alpha_t^H \in \mathbb{R}^{k \times 1}$ by solving Eq. 6 with LARS-Lasso [60] algorithm.
4. Update \mathbf{B}_t^H and \mathbf{C}_t^H :
 $\mathbf{B}_t^H = \sum_{i=1}^t \alpha_i^H (\alpha_i^H)^T = \mathbf{B}_{t-1}^H + \alpha_t^H (\alpha_t^H)^T$,
 $\mathbf{C}_t^H = \sum_{i=1}^t \mathbf{x}_i^H (\alpha_i^H)^T = \mathbf{C}_{t-1}^H + \mathbf{x}_t^H (\alpha_t^H)^T$.
5. Dictionary update:
For $t = 1$ to T **do**
 $\mathbf{d}_{j,t}^H = \mathbf{d}_{j,t-1}^H - \frac{1}{\mathbf{B}_j^H(j,j)} \left(\hat{\mathbf{D}}_{j,t}^H \mathbf{b}_{j,t}^H - \mathbf{c}_{j,t}^H \right) - 2\lambda_2 \sigma \mathbf{W}_j \mathbf{W}_j^T \mathbf{d}_{j,t-1}^H$,
End For
6. Obtain the discriminant dictionary $\mathbf{D}_t^H = [\mathbf{d}_{1,t}^H, \mathbf{d}_{2,t}^H, \dots, \mathbf{d}_{k,t}^H]$ for the current iteration.
7. **End For**
8. **Return:** The learned dictionary $\mathbf{D}^H = \mathbf{D}_T^H$.

salient dictionary, nonsalient image patches obtain their SR coefficients with high energy; conversely, saliency image patches obtain their SR coefficients with lower energy. This is because of the saliency dictionary has high contrast with nonsaliency image patches, and the saliency image patches have low contrast. On the basis of this observation, we define the saliency measure of a pixel as

$$S_{\mathbf{A}(i)} = 1 - \exp \left(- \frac{\|\alpha_i^N\|_2^2 - \|\alpha_i^P\|_2^2}{2\eta_{\mathbf{A}}^2} \right), \quad (13)$$

where α_i^N and α_i^P respectively represent the representation coefficients the image patch centered on a pixel i by the discriminant dictionary, $\eta_{\mathbf{A}}$ is a scalar parameter, and the experimental setting is 1.

3.3.2. Saliency measurement based on reconstruction error

Reconstruction error is widely used in saliency detection based on SR. Generally speaking, the image patch has a larger relative reconstruction error for the discriminant dictionary, so it will have a greater saliency value. Therefore, we define the saliency measure of pixels based on SR coefficients

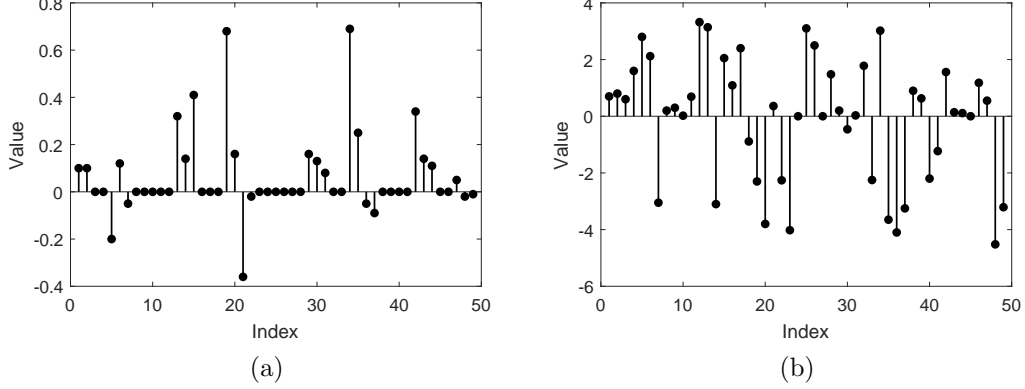


Figure 2: A salient dictionary used to represent the comparison of the representation coefficients of salient patches and nonsalient patches. (a) Representation coefficients of salient patches. (b) Representation coefficients of nonsalient patches.

as

$$S_{\mathbf{R}(i)} = 1 - \exp \left(- \frac{\min_{\alpha_i^N} \|x_i - D^N \alpha_i^N\|_{2,1} - \min_{\alpha_i^P} \|x_i - D^N \alpha_i^P\|_{2,1}}{2\eta_{\mathbf{R}}^2} \right), \quad (14)$$

where x_i is the image patch centered on a pixel i , D^N and D^P nonsalient dictionary and salient dictionary respectively, α_i^N and α_i^P represent the representation coefficients obtained by the discriminant dictionary, $\eta_{\mathbf{R}}$ is a scalar parameter, the experimental setting is 1.

3.4. Salient image fusion

In the field of information fusion, information fusion methods can achieve better results than a single information source according to appropriate fusion criteria. The traditional pixel-level salient image fusion method generates a fused image through the weighted sum of multisalient maps, which can be expressed as

$$S_{fused}(x, y) = \sum_{n=1}^N W_n(x, y) S_n(x, y), \quad (15)$$

where N is the number of salient images to be fused, $S_n(x, y)$ is the pixel intensity of the n -th salient image at (x, y) , and $W_n(x, y)$ is the weight of

the importance of pixel $S_n(x, y)$ at (x, y) . Therefore, the key to fusion is how to design a reasonable weight.

According to the above, on the basis of the observation of the cumulative histogram of pixel intensity (the histogram integral along the pixel intensity axis), we propose a weight function to suppress the background region and highlight the foreground region in the fusion of salient images.

Fig. 3 is an example of a cumulative histogram of a coefficient representation map, a reconstruction error map to be fused, and an optimised fusion map. The cumulative histogram in the optimised fusion map increases sharply at the beginning; in other words, there are relatively many pixels in this interval, and the intensity of the pixels around it has a small change with a larger gradient than that of the salient image to be fused. In the middle region of pixel intensity (0.2 to 0.8), the cumulative histogram changes slowly, indicating that there are relatively few pixels in this region, and the pixel intensity around it has a greater change that has a smaller gradient compared with the salient image to be fused. The analysis of the interval where the pixel intensity is close to 1 also has the same rule as above. Therefore, when the pixels are in the range of a cumulative histogram with a large gradient, the pixels need to be given more weight in image fusion.

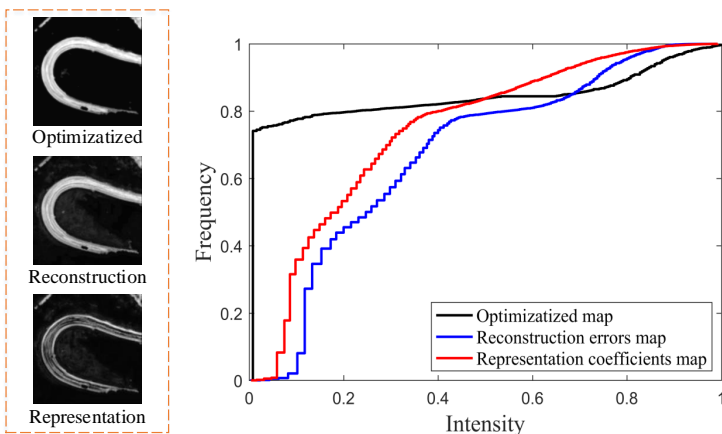


Figure 3: Cumulative histogram comparison of different salient maps.

Formally, we can express this observation as

$$W_n(x, y) = \frac{Grad_n(I_n(x, y))}{\sum_{n=1}^N Grad_n(I_n(x, y)) + \varphi}, \quad (16)$$

Where φ is to avoid a very small positive number with zero denominators, and $Grad_n(I_n(x, y))$ is the gradient of the cumulative histogram at pixel intensity $I_n(x, y)$. Because the cumulative histogram is the statistical information of all pixels, the gradient in Eq. 16 is not the local gradient around the pixel; we call it the global gradient. Using the weights obtained above, we can fuse several salient maps obtained by representation coefficients and reconstruction errors according to Eq. 15.

4. Experiments

In this section, we first introduce the constructed dataset for road saliency detection in RS images and then explain the dictionary training strategy, evaluation metrics, and implementation details. Finally, we compare the proposed method with nine state-of-the-art methods.

4.1. Experimental setup

4.1.1. Dataset

To the best of our knowledge, no publicly available dataset of optical RS images can be used for road detection. Therefore, we collected 300 optical RS images to build a dataset for road saliency detection, which we called 2RSOD, and manually pixel-wise annotated each image. Most of the original optical RS images were collected on Google Earth, and others were collected from existing optical RS image datasets, including DOTA dataset [61], NWPU VHR-10 dataset [62]. This 2RSOD was challenging because the spatial resolutions of the image were diverse, including 300×300 , 500×500 and 1024×1024 . Also, the background was complicated and cluttered, including some buildings, trees, rivers, and shadows. The sizes, numbers, and shapes of the salient objects were variable. Some of the sample images in the constructed 2RSOD dataset are shown in Fig. 4.

4.1.2. Evaluation metrics

To quantitatively evaluate the performance of various methods, we adopted six evaluation metrics. Table 2 summarises these metrics.

4.1.3. Parameter setting

All parameter settings related to our experiment are summarised in Table 3. To evaluate the performance of the saliency detection algorithm, for the dataset we randomly select 240 images as the training set and the remaining

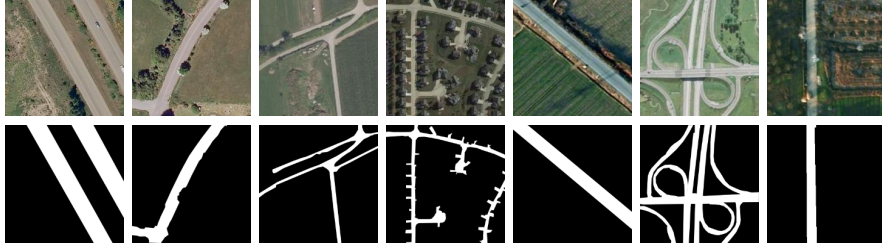


Figure 4: Sample images from the constructed 2RSOD dataset. The first row is the optical RS images. The second row is the pixel-wise annotation.

Table 2: Summary of evaluation metrics

Metric	Mathematical Expression
Precision-Recall (PR) \uparrow	$Precision (P) : \frac{ S \cap G }{ S }, Recll (R) : \frac{ S \cap G }{ G }$
F-measure(Fm) \uparrow	$F_{\beta} = (1 + \beta^2) \frac{P * R}{\beta^2 P + R}, \beta^2 = 0.3$
S-measure(Sm) \uparrow	$S = \alpha * S_0 + (1 - \alpha) * S_r, \alpha = 0.5$
E-measure(Em) \uparrow	$E = \frac{1}{W * H} \sum_{i=1}^W \sum_{j=1}^H \phi_{FM}(i, j)$
Adaptive threshold (Fm), (Em) \uparrow	$Thr = \frac{1}{W * H} \sum_{i=1}^W \sum_{j=1}^H S(i, j)$
Mean absolute error (MAE) \downarrow	$MEA = \frac{1}{W * H} \sum_{i=1}^W \sum_{j=1}^H S(i, j) - G(i, j) $
Note: \uparrow means the bigger the better, and \downarrow means the smaller the better.	
S :salient image	S_o :target perception structure [63]
G :corresponding annotation map	ϕ :enhanced contrast matrix [64]
$ \bullet $:calculates the number of nonzero entries	W :width of the image
S_r :similarity measurement of the region[63]	H :height of the image

60 images as the testing set. For dictionary learning of our proposed CWDL algorithm, we sampled 480 saliency and nonsaliency image patches of size 80×80 from the training set as training patches. In the process of dictionary training, according to the empirical setting in article [19], we down-sampled the training patch into an image patch of size 16×16 as the input for dictionary training, so that the number of pixels m of the learned dictionary atom is 256, and the number of atoms in the dictionary k was set to $4 \times m$. In Eq. 5, the regularisation parameter λ_1 is set to $1.2/\sqrt{m}$ for weighing the reconstruction error and sparsity, and the learning rate σ was set to 0.02 in dictionary learning Eq. 12 to obtain a better discrimination dictionary. Also, we used various values $\lambda_0 = 0.001, \lambda_1 = 0.005, \lambda_2 = 0.01, \lambda_3 = 0.02, \lambda_4 = 0.03, \lambda_5 = 0.04, \lambda_6 = 0.05, \lambda_7 = 0.06, \lambda_8 = 0.07, \lambda_9 = 0.09, \lambda_{10} = 0.1$ for testing according to λ_2 . The experimental results are shown in Fig. 5, according to which the parameter λ_2 in Eq. 12 was adjusted to 0.05.

Table 3: Parameter setting in our method

Process	Parameter Description	Value
Dictionary learning	Training patch size	16×16
	Dictionary atom size m	256×1
	Number of atoms in the dictionary k	1×1024
	Regularisation parameter λ_1	0.02
	Regularisation parameter λ_2	0.02
Saliency detection	Scalar parameter $\eta_{\mathbf{A}}$	1
	Scalar parameter $\eta_{\mathbf{R}}$	1
	Positive value φ	0.001

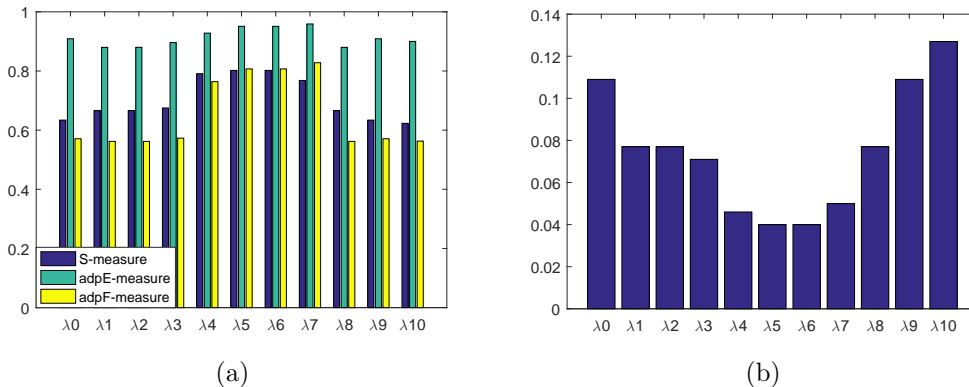


Figure 5: Quantitative comparison of various values λ_2 . (a) S-measure, adaptive F-measure and E-measure values. (b) MAE values.

4.2. Verification and analysis

In this subsection, we first use the 2RSOD dataset to show the effectiveness of the LCWA-based method, then compare our proposed method with advanced methods, and finally analyze some failure examples in our method.

4.2.1. Effectiveness analysis based on LCWA method

In this subsection, we analyze and verify the effectiveness of the proposed LCWA-based saliency detection method on the 2RSOD dataset from the following four aspects:

A. Effectiveness of contrast-weighted terms

The contrast-weighted term in Eq. 7 was used to optimise the atoms update during the learning process of the discriminant dictionary. We removed the contrast-weighted term (N-CW) to verify its effectiveness, as shown in

N-CW in Fig. 6 (a).

B. Effectiveness of constructing a discriminant dictionary

Discriminant dictionaries have their own features for the SR of images. To verify the effectiveness of the discriminant dictionary for saliency detection, we used the single salient dictionary (S-SD) or single nonsalient dictionary (S-NSD) for saliency detection.

C. The validity of significance measures for joint representation coefficients and reconstruction errors

To improve the expression of outliers in the coefficients of the SR, we combined representation coefficient and reconstruction errors as a measure of saliency detection. To verify the effectiveness of the joint saliency measure, we used the single representation coefficient (S-RC) and the single reconstruction error (S-RE) as the saliency measurements.

D. Effectiveness of saliency map fusion method based on global gradient optimization

To improve the use of correct information in multiple salient maps, we proposed a saliency map fusion method based on global gradient optimisation. We compared the saliency of this proposed optimisation method with the equal weight fusion (EWF) method as a verification of the effectiveness of the proposed method.

Fig. 6 shows that many evaluation metrics of the proposed saliency detection method based on LCWA are superior to those of the above effectiveness verification method. The figure also shows the importance and contribution of the various parts that make up the proposed method.

4.2.2. Comparison with state-of-the-art methods

We compared the proposed method with nine salient object detection methods on the 2RSOD dataset, including LPS [65], HDCT [66], BFS [67], DSG [68], WMR [69], methods related to SR WLRR [70], SMD [32], RSR-LC [31], and RDR [33]. All results were either generated by the source code or provided by the author.

A. Visual comparison

Fig. 7 shows some results obtained by these methods. As shown in the figure, most of the methods mentioned in this paper had poor detection effects on the 2RSOD dataset. Through careful comparison, we found that the proposed contrast method performed better on saliency detection for images with simple backgrounds and prominent foregrounds (for example, the third and sixth rows in Fig. 7). However, for the image with a complex

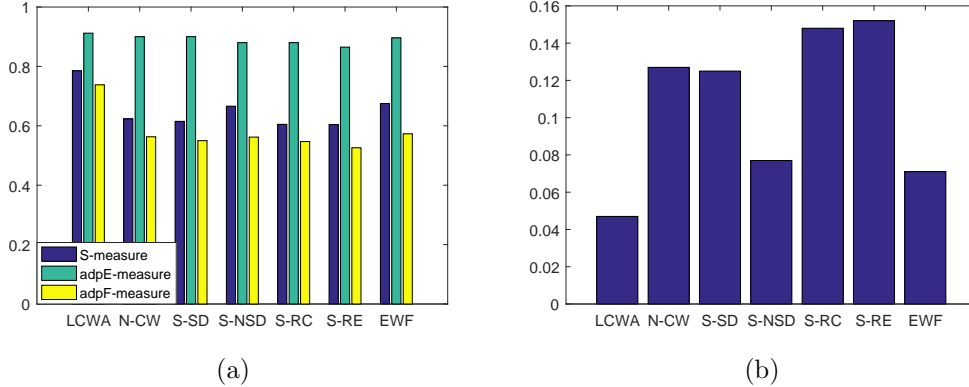


Figure 6: Quantitative comparison of various verification methods. (a) S-measure, adaptive F-measure and E-measure values. (b) MAE values.

backgrounds (for example, the second row and the eighth row in Fig. 7), that contain shadows, buildings, and so on, these methods do not have satisfactory results. Moreover, because most of the saliency road regions of the images in the 2RSOD dataset were linked to image boundaries, the accuracy of saliency detection of these methods based on boundary priors (for example, BFS [67], WMR [69], WLRR [69], SMD [32], RSR-LC [31], RDR [33]) were also affected. In contrast, the proposed method could separate the salient object from the background well and had good detection results for images with complex scenes or similar foreground and background.

B. Quantitative comparison

Fig. 8 shows the quantitative results of various methods, complying with those subjective results mentioned in Fig. 7. For the six evaluation metrics, the proposed method was found superior to other methods. As shown in Fig. 8(b), the proposed method took the largest F-measure score in the 2RSOD dataset, which indicates that the salient value of the foreground regions obtained by this method is higher and the background regions are small. It also shows that this method is more robust to the separation of thresholds. However, as shown in Fig. 8(c), the largest S-measure score was obtained by the proposed method, which indicates that it had the highest structural similarity compared with other detection methods. Also, in Fig. 8(d), the proposed method had the lowest mean absolute error score, which means that the method was closest to that of the manually labeled graph. In

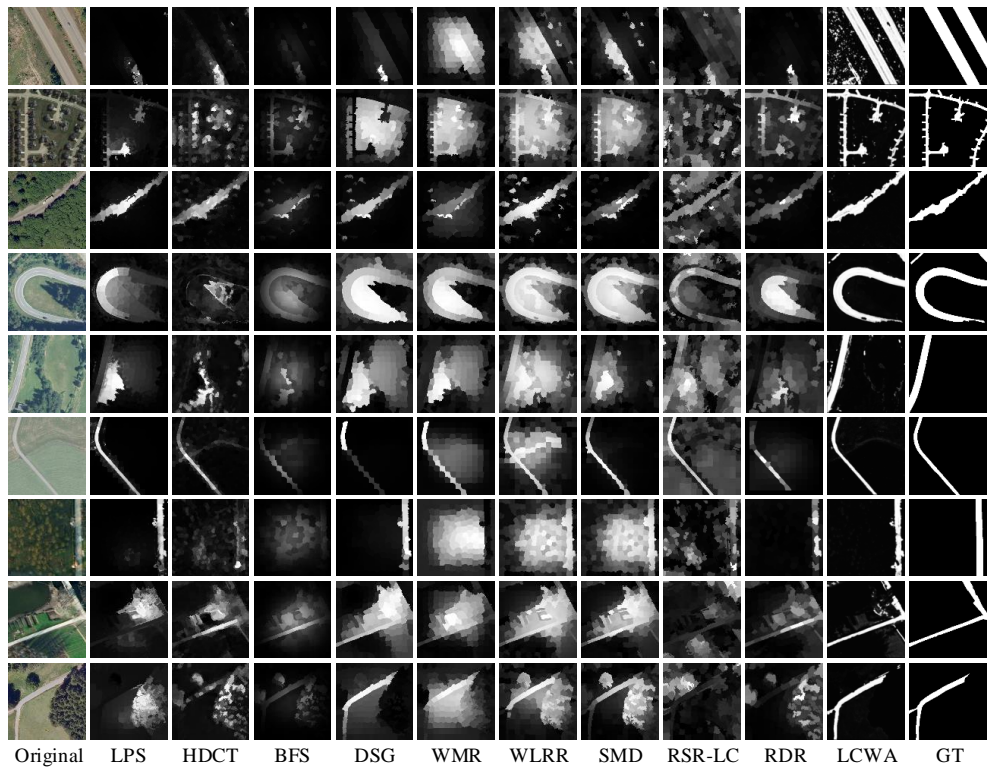


Figure 7: Visual comparisons of various methods (GT is ground truth).

Table 4: Average execution time of several methods (image size: 300×300)

Method	Ours	LPS[65]	HDCT[66]	BFS[67]	DSG[68]	WMR[69]	WLRR[70]	SMD[32]	SRS-LC[31]	RDR[33]
Time(s)	4.87	2.21	5.12	5.31	0.83	1.56	1.16	0.91	3.32	2.48

particular, the method proposed in this paper was significantly better than the saliency detection method related to SR.

C. Computational complexity comparison

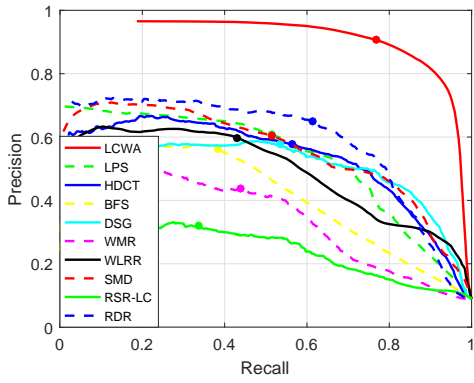
To show the computational efficiency of the proposed method, we listed the average execution time of several state-of-the-art methods and the proposed method on the 2RSOD dataset. These methods were all run in MATLAB2016 on a PC with an Intel Core i7-7700 3.60 GHz CPU. As shown in Table 4, our method was less efficient than most methods and only slightly faster than the HDCT [66] and BFS [67] methods. This is because the proposed method was calculated based on pixel-by-pixel image patches, whereas the contrasting methods are mostly based on superpixels.

4.2.3. Failure cases

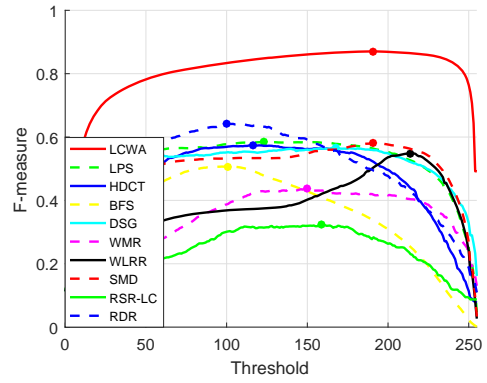
Although the proposed method could accurately detect most road salient regions, there were still some limitations. Fig. 9 shows that when the image contained regions similar to the appearance of the road (such as roofs, or farmland), our proposed method incorrectly marked the background regions as the foreground. Also, the places where the road salient regions would be interrupted are shown in the third column of Fig. 9, which was inconsistent with the fact that the road had connectivity. On the other hand, the saliency of the road should be regional and overall, but as shown in the first and second columns of Fig. 9, there were many scattered points with high saliency values in the inspection results. Through the above analysis, for future work we can develop a more robust dictionary construction method and combine the semantic information of the image and the feature information of the road (such as texture and shape) to overcome these problems.

5. Conclusion

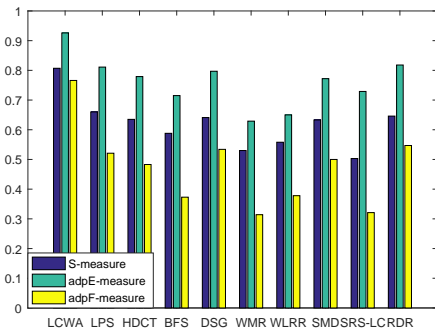
This paper proposes a novel method for road saliency detection in RS images. First, the contrast weight term is introduced into the dictionary learning process, which was used to build a discriminant dictionary based



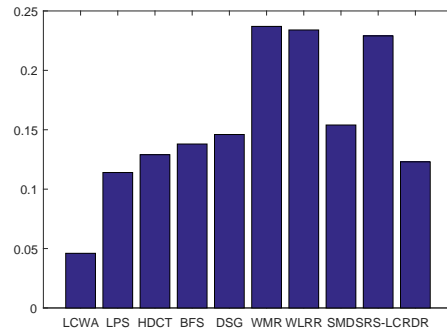
(a)



(b)



(c)



(d)

Figure 8: Comparison of our method with different methods. (a) PR curve. (b) F-measure curve. (c) S-measure, adaptive F-measure and E-measure values. (d) MAE value. The point in the (a) and (b) curve represents the maximum value.

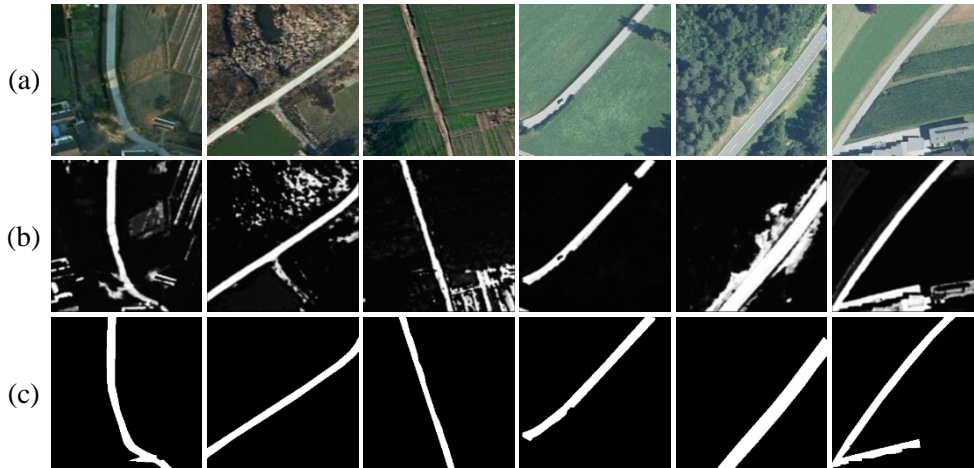


Figure 9: Failure cases of proposed method. (a) Original images. (b) Saliency maps obtained by the proposed method. (c) Ground truth.

on the learning contrast-weighted atom. Then, in accordance with the characteristics of online dictionary learning, we proposed an online discriminant dictionary learning algorithm based on contrast weight to solve the optimisation formula. Using the discriminant dictionary, we combined the representation coefficients and reconstruction errors of image patches as saliency detection metrics to generate multiple saliency maps. For multiple saliency maps, we propose a saliency map fusion method based on global gradient optimisation to improve the use of effective information in saliency maps. Experimental results show that our method is superior to most of the current state-of-the-art methods.

6. Acknowledgment

This research was supported by a grant from the Sichuan Major Science and Technology Special Foundation (No.2018GZDZX0017).

References

- [1] A. Borji, L. Itti, State-of-the-art in visual attention modeling, *IEEE transactions on pattern analysis and machine intelligence* 35 (1) (2012) 185–207.

- [2] J. M. Wolfe, T. S. Horowitz, What attributes guide the deployment of visual attention and how do they do it?, *Nature reviews neuroscience* 5 (6) (2004) 495.
- [3] S. K. Mannan, C. Kennard, M. Husain, The role of visual salience in directing eye movements in visual object agnosia, *Current biology* 19 (6) (2009) R247–R248.
- [4] A. Borji, M.-M. Cheng, H. Jiang, J. Li, Salient object detection: A benchmark, *IEEE transactions on image processing* 24 (12) (2015) 5706–5722.
- [5] D.-P. Fan, M.-M. Cheng, J.-J. Liu, S.-H. Gao, Q. Hou, A. Borji, Salient objects in clutter: Bringing salient object detection to the foreground, in: *Proceedings of the European Conference on Computer Vision (ECCV)*, 2018, pp. 186–202.
- [6] A. Borji, D. N. Sihite, L. Itti, Quantitative analysis of human-model agreement in visual saliency modeling: A comparative study, *IEEE Transactions on Image Processing* 22 (1) (2012) 55–69.
- [7] M.-M. Cheng, J. Warrell, W.-Y. Lin, S. Zheng, V. Vineet, N. Crook, Efficient salient region detection with soft image abstraction, in: *Proceedings of the IEEE International Conference on Computer vision*, 2013, pp. 1529–1536.
- [8] J.-X. Zhao, J.-J. Liu, D.-P. Fan, Y. Cao, J. Yang, M.-M. Cheng, Egnet: Edge guidance network for salient object detection, in: *Proceedings of the IEEE International Conference on Computer Vision*, 2019, pp. 8779–8788.
- [9] D.-P. Fan, W. Wang, M.-M. Cheng, J. Shen, Shifting more attention to video salient object detection, in: *Proceedings of the IEEE Conference on Computer Vision and Pattern Recognition*, 2019, pp. 8554–8564.
- [10] Q. Fan, C. Qi, Saliency detection based on global and local short-term sparse representation, *Neurocomputing* 175 (2016) 81–89.
- [11] M.-M. Cheng, Z. Zhang, W.-Y. Lin, P. Torr, Bing: Binarized normed gradients for objectness estimation at 300fps, in: *Proceedings of the*

- IEEE conference on computer vision and pattern recognition, 2014, pp. 3286–3293.
- [12] W. Wang, J. Shen, L. Shao, Consistent video saliency using local gradient flow optimization and global refinement, *IEEE Transactions on Image Processing* 24 (11) (2015) 4185–4196.
 - [13] W. Wang, J. Shen, R. Yang, F. Porikli, Saliency-aware video object segmentation, *IEEE transactions on pattern analysis and machine intelligence* 40 (1) (2017) 20–33.
 - [14] L. Zhang, Y. Wang, X. Li, S. Wang, Region-of-interest extraction based on spectrum saliency analysis and coherence-enhancing diffusion model in remote sensing images, *Neurocomputing* 207 (2016) 630–644.
 - [15] W. Feng, H. Sui, J. Tu, W. Huang, K. Sun, A novel change detection approach based on visual saliency and random forest from multi-temporal high-resolution remote-sensing images, *International journal of remote sensing* 39 (22) (2018) 7998–8021.
 - [16] L. Zhang, J. Zhang, A new saliency-driven fusion method based on complex wavelet transform for remote sensing images, *IEEE Geoscience and remote sensing letters* 14 (12) (2017) 2433–2437.
 - [17] A. Garcia-Diaz, V. Leboran, X. R. Fdez-Vidal, X. M. Pardo, On the relationship between optical variability, visual saliency, and eye fixations: A computational approach, *Journal of vision* 12 (6) (2012) 17–17.
 - [18] B. A. Olshausen, D. J. Field, Sparse coding of sensory inputs, *Current opinion in neurobiology* 14 (4) (2004) 481–487.
 - [19] J. Mairal, F. Bach, J. Ponce, G. Sapiro, Online dictionary learning for sparse coding, in: *Proceedings of the 26th annual international conference on machine learning*, ACM, 2009, pp. 689–696.
 - [20] Q. Wei, J. Bioucas-Dias, N. Dobigeon, J.-Y. Tournier, Hyperspectral and multispectral image fusion based on a sparse representation, *IEEE Transactions on Geoscience and Remote Sensing* 53 (7) (2015) 3658–3668.

- [21] J. Cao, K. Zhang, M. Luo, C. Yin, X. Lai, Extreme learning machine and adaptive sparse representation for image classification, *Neural networks* 81 (2016) 91–102.
- [22] W. Dong, L. Zhang, G. Shi, X. Li, Nonlocally centralized sparse representation for image restoration, *IEEE transactions on Image Processing* 22 (4) (2012) 1620–1630.
- [23] X. Li, H. Lu, L. Zhang, X. Ruan, M.-H. Yang, Saliency detection via dense and sparse reconstruction, in: *Proceedings of the IEEE International Conference on Computer Vision*, 2013, pp. 2976–2983.
- [24] Y. Zhang, X. Wang, X. Xie, Y. Li, Salient object detection via recursive sparse representation, *Remote Sensing* 10 (4) (2018) 652.
- [25] N. Bruce, J. Tsotsos, Saliency based on information maximization, in: *Advances in neural information processing systems*, 2006, pp. 155–162.
- [26] X. Hou, L. Zhang, Dynamic visual attention: Searching for coding length increments, in: *Advances in neural information processing systems*, 2009, pp. 681–688.
- [27] B. Han, H. Zhu, Y. Ding, Bottom-up saliency based on weighted sparse coding residual, in: *Proceedings of the 19th ACM international conference on Multimedia*, ACM, 2011, pp. 1117–1120.
- [28] J. Yan, M. Zhu, H. Liu, Y. Liu, Visual saliency detection via sparsity pursuit, *IEEE Signal Processing Letters* 17 (8) (2010) 739–742.
- [29] X. Shen, Y. Wu, A unified approach to salient object detection via low rank matrix recovery, in: *2012 IEEE Conference on Computer Vision and Pattern Recognition*, IEEE, 2012, pp. 853–860.
- [30] Y. Wei, F. Wen, W. Zhu, J. Sun, Geodesic saliency using background priors, in: *European conference on computer vision*, Springer, 2012, pp. 29–42.
- [31] L. Yi, Z. Qiang, H. Jungong, W. Long, Salient object detection employing robust sparse representation and local consistency, *Image and Vision Computing* 69 (2018) 155–167.

- [32] H. Peng, B. Li, H. Ling, W. Hu, W. Xiong, S. J. Maybank, Salient object detection via structured matrix decomposition, *IEEE transactions on pattern analysis and machine intelligence* 39 (4) (2016) 818–832.
- [33] H. Xiao, W. Ren, W. Wang, Y. Liu, M. Zhang, Salient object detection via robust dictionary representation, *Multimedia Tools and Applications* 77 (3) (2018) 3317–3337.
- [34] H. Lu, X. Li, L. Zhang, X. Ruan, M.-H. Yang, Dense and sparse reconstruction error based saliency descriptor, *IEEE Transactions on Image Processing* 25 (4) (2016) 1592–1603.
- [35] J. Ling, K. Zhang, Y. Zhang, D. Yang, Z. Chen, A saliency prediction model on 360 degree images using color dictionary based sparse representation, *Signal Processing: Image Communication* 69 (2018) 60–68.
- [36] F. Perazzi, P. Krähenbühl, Y. Pritch, A. Hornung, Saliency filters: Contrast based filtering for salient region detection, in: *2012 IEEE conference on computer vision and pattern recognition*, IEEE, 2012, pp. 733–740.
- [37] M. Xu, L. Jiang, Z. Ye, Z. Wang, Bottom-up saliency detection with sparse representation of learnt texture atoms, *Pattern Recognition* 60 (2016) 348–360.
- [38] W. Wang, J. Shen, J. Xie, M.-M. Cheng, H. Ling, A. Borji, Revisiting video saliency prediction in the deep learning era, *IEEE transactions on pattern analysis and machine intelligence* (2019).
- [39] W. Wang, J. Shen, L. Shao, F. Porikli, Correspondence driven saliency transfer, *IEEE Transactions on Image Processing* 25 (11) (2016) 5025–5034.
- [40] W. Wang, J. Shen, Y. Yu, K.-L. Ma, Stereoscopic thumbnail creation via efficient stereo saliency detection, *IEEE transactions on visualization and computer graphics* 23 (8) (2016) 2014–2027.
- [41] X. Sun, H. Yao, R. Ji, P. Xu, X. Liu, S. Liu, Saliency detection based on short-term sparse representation, in: *2010 IEEE International Conference on Image Processing*, IEEE, 2010, pp. 1101–1104.

- [42] Y. Li, Y. Zhou, L. Xu, X. Yang, J. Yang, Incremental sparse saliency detection, in: 2009 16th IEEE International Conference on Image Processing (ICIP), IEEE, 2009, pp. 3093–3096.
- [43] S. Wang, M. Wang, S. Yang, K. Zhang, Salient region detection via discriminative dictionary learning and joint bayesian inference, *IEEE Transactions on Circuits and Systems for Video Technology* 28 (5) (2017) 1116–1129.
- [44] Y. Liu, J. Han, Q. Zhang, L. Wang, Salient object detection via two-stage graphs, *IEEE Transactions on Circuits and Systems for Video Technology* 29 (4) (2018) 1023–1037.
- [45] X. Yao, J. Han, L. Guo, S. Bu, Z. Liu, A coarse-to-fine model for airport detection from remote sensing images using target-oriented visual saliency and crf, *Neurocomputing* 164 (2015) 162–172.
- [46] E. Li, S. Xu, W. Meng, X. Zhang, Building extraction from remotely sensed images by integrating saliency cue, *IEEE Journal of Selected Topics in Applied Earth Observations and Remote Sensing* 10 (3) (2016) 906–919.
- [47] Z. Liu, D. Zhao, Z. Shi, Z. Jiang, Unsupervised saliency model with color markov chain for oil tank detection, *Remote Sensing* 11 (9) (2019) 1089.
- [48] C. Dong, J. Liu, F. Xu, Ship detection in optical remote sensing images based on saliency and a rotation-invariant descriptor, *Remote Sensing* 10 (3) (2018) 400.
- [49] L. Ma, B. Du, H. Chen, N. Q. Soomro, Region-of-interest detection via superpixel-to-pixel saliency analysis for remote sensing image, *IEEE Geoscience and remote sensing letters* 13 (12) (2016) 1752–1756.
- [50] H. Peng, B. Li, W. Xiong, W. Hu, R. Ji, Rgb-d salient object detection: A benchmark and algorithms, in: *European conference on computer vision*, Springer, 2014, pp. 92–109.
- [51] D. Feng, N. Barnes, S. You, C. McCarthy, Local background enclosure for rgb-d salient object detection, in: *Proceedings of the IEEE Conference on Computer Vision and Pattern Recognition*, 2016, pp. 2343–2350.

- [52] R. Ju, L. Ge, W. Geng, T. Ren, G. Wu, Depth saliency based on anisotropic center-surround difference, in: 2014 IEEE International Conference on Image Processing (ICIP), IEEE, 2014, pp. 1115–1119.
- [53] L. Qu, S. He, J. Zhang, J. Tian, Y. Tang, Q. Yang, Rgb-d salient object detection via deep fusion, *IEEE Transactions on Image Processing* 26 (5) (2017) 2274–2285.
- [54] H. Chen, Y. Li, Progressively complementarity-aware fusion network for rgb-d salient object detection, in: Proceedings of the IEEE Conference on Computer Vision and Pattern Recognition, 2018, pp. 3051–3060.
- [55] J.-X. Zhao, Y. Cao, D.-P. Fan, M.-M. Cheng, X.-Y. Li, L. Zhang, Contrast prior and fluid pyramid integration for rgb-d salient object detection, in: Proceedings of the IEEE Conference on Computer Vision and Pattern Recognition (CVPR), 2019.
- [56] Y. Piao, W. Ji, J. Li, M. Zhang, H. Lu, Depth-induced multi-scale recurrent attention network for saliency detection, in: Proceedings of the IEEE International Conference on Computer Vision, 2019, pp. 7254–7263.
- [57] D.-P. Fan, Z. Lin, J.-X. Zhao, Y. Liu, Z. Zhang, Q. Hou, M. Zhu, M.-M. Cheng, Rethinking rgb-d salient object detection: Models, datasets, and large-scale benchmarks, *arXiv preprint arXiv:1907.06781* (2019).
- [58] M.-M. Cheng, N. J. Mitra, X. Huang, P. H. Torr, S.-M. Hu, Global contrast based salient region detection, *IEEE Transactions on Pattern Analysis and Machine Intelligence* 37 (3) (2014) 569–582.
- [59] M. R. Osborne, B. Presnell, B. A. Turlach, A new approach to variable selection in least squares problems, *IMA journal of numerical analysis* 20 (3) (2000) 389–403.
- [60] S. J. Wright, Coordinate descent algorithms, *Mathematical Programming* 151 (1) (2015) 3–34.
- [61] G.-S. Xia, X. Bai, J. Ding, Z. Zhu, S. Belongie, J. Luo, M. Datcu, M. Pelillo, L. Zhang, Dota: A large-scale dataset for object detection in aerial images, in: Proceedings of the IEEE Conference on Computer Vision and Pattern Recognition, 2018, pp. 3974–3983.

- [62] G. Cheng, P. Zhou, J. Han, Learning rotation-invariant convolutional neural networks for object detection in vhr optical remote sensing images, *IEEE Transactions on Geoscience and Remote Sensing* 54 (12) (2016) 7405–7415.
- [63] D.-P. Fan, M.-M. Cheng, Y. Liu, T. Li, A. Borji, Structure-measure: A new way to evaluate foreground maps, in: *Proceedings of the IEEE international conference on computer vision*, 2017, pp. 4548–4557.
- [64] D.-P. Fan, C. Gong, Y. Cao, B. Ren, M.-M. Cheng, A. Borji, Enhanced-alignment Measure for Binary Foreground Map Evaluation, in: *International Joint Conference on Artificial Intelligence (IJCAI)*, 2018, pp. 698–704, <http://dpfan.net/e-measure/>.
- [65] H. Li, H. Lu, Z. Lin, X. Shen, B. Price, Inner and inter label propagation: salient object detection in the wild, *IEEE Transactions on Image Processing* 24 (10) (2015) 3176–3186.
- [66] J. Kim, D. Han, Y.-W. Tai, J. Kim, Salient region detection via high-dimensional color transform and local spatial support, *IEEE transactions on image processing* 25 (1) (2015) 9–23.
- [67] J. Wang, H. Lu, X. Li, N. Tong, W. Liu, Saliency detection via background and foreground seed selection, *Neurocomputing* 152 (2015) 359–368.
- [68] L. Zhou, Z. Yang, Z. Zhou, D. Hu, Salient region detection using diffusion process on a two-layer sparse graph, *IEEE Transactions on Image Processing* 26 (12) (2017) 5882–5894.
- [69] X. Zhu, C. Tang, P. Wang, H. Xu, M. Wang, J. Chen, J. Tian, Saliency detection via affinity graph learning and weighted manifold ranking, *Neurocomputing* 312 (2018) 239–250.
- [70] C. Tang, P. Wang, C. Zhang, W. Li, Salient object detection via weighted low rank matrix recovery, *IEEE Signal Processing Letters* 24 (4) (2016) 490–494.